Supplemental figures

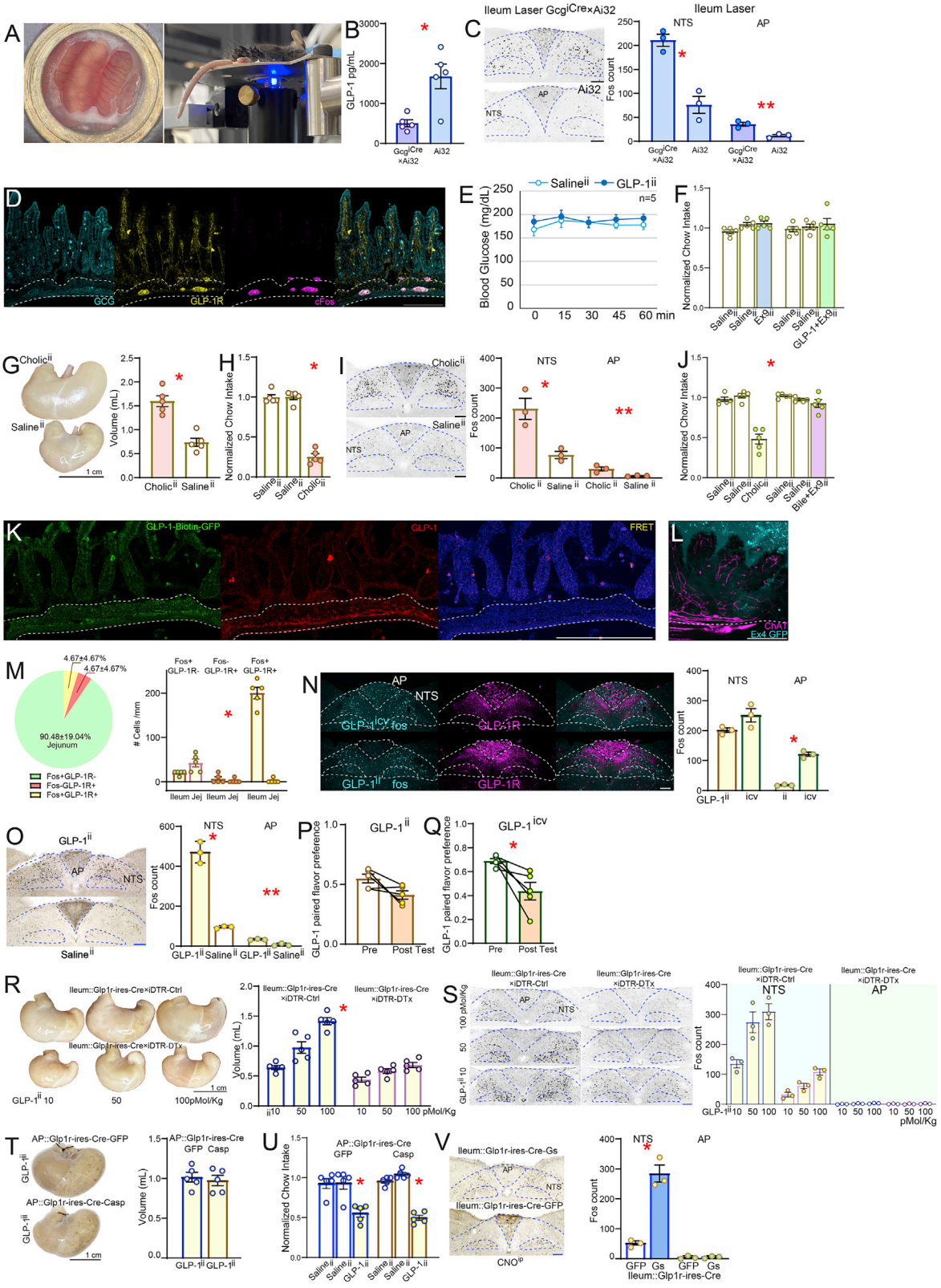

(legend on next page)

Figure S1. Ileal GLP-1 induces gastric and anorectic effects via enteric neurons, related to Figure 1

(A) Representative image of the intravital window placed over the lower abdominal area of Gcg^{iCre}×Ai32 mice for *in vivo* optogenetic stimulation of (GCG+) L cells. During experiments, mice were under light anesthesia.

(B) Ileum GLP-1 concentrations were significantly depleted after 1-h-long optogenetic stimulation in Gcg^{iCre}×Ai32 mice compared with Ai32 littermate controls. The results show that optogenetic stimulation was effective in inducing GLP-1 secretion from L cells *in vivo*. 2-sample t test T(8) = 3.652, * p = 0.006.

(C) *In vivo* optogenetic stimulation of L cells in the distal ileum induced neuronal Fos expression in *nucleus tractus solitarius* (NTS) and *area postrema* (AP); Gcg^{iCre}×Ai32 mice versus Ai32 littermate controls; 2-sample t test T(4) = 6.209, * p = 0.003 (NTS); T(4) = 5.052, ** p = 0.007 (AP).

(D) *In vivo* optogenetic stimulation of L cells in the distal ileum of Gcg^{iCre}×Ai32 mice induced Fos expression (magenta) in the submucosal and myenteric GLP-1R+ cells (yellow). L cells (GCG+) are shown in cyan. Dotted lines delimit the ileal myenteric layer.

(E) Intra-ileal infusions of GLP-1 (GLP-1^{ii}) do not affect blood glucose levels compared with intra-ileal saline (Saline^{ii}) in food-restricted mice: GLP-1^{ii} versus Saline^{ii}, two-way RM-ANOVA, infusate × time F(4,32) = 1.334, p = 0.279.

(F) In a within-subject design, intra-ileal infusions of the GLP-1R antagonist Exendin9-39 (Ex9–39^{ii}) did not affect intake but completely blocked the anorectic effects of GLP-1^{ii}, 1 h-food intake, two-way RM-ANOVA, treatment (Saline^{ii} baseline versus peptide) × condition (Ex9–39^{ii} versus [GLP-1+Ex9-39]^{ii}), F(2,16) = 0.264, p = 0.772.

(G) Intra-ileal infusions of the bile constituent cholic acid (Cholic^{ii}, 400 mg/kg) expanded gastric volumes by ~100% compared with intra-ileal saline (Saline^{ii}); left, representative dissected stomachs, Scale bars, 1 cm; right: volume of dissected stomach (in mL); Cholic^{ii} versus Saline^{ii}, 2-sample t test T(8) = 6.069, * p < 0.001.

(H) Cholic^{ii} decreases food intake by ~60% over 1 h, Cholic^{ii} versus Saline^{ii} baseline, one-way RM-ANOVA F(2,8) = 112.4, * p < 0.001.

(I) Cholic^{ii} induces Fos expression in NTS and AP, Cholic^{ii} versus Saline^{ii}; NTS, 2-sample t test T(4) = 4.142, * p = 0.014; AP, T(4) = 3.318, ** p = 0.029.

(J) Intra-ileal infusions of the GLP-1R antagonist Exendin9-39 blocked the anorectic effects of intra-ileal infusions of cholic acids, same analysis as in (F), 1 h-food intake F(2,8) = 18.076, * p = 0.001.

(K) Confocal imaging of tissue collected 10 min after intra-ileal infusions of N-terminal biotin-conjugated-GLP-1(7-36), left: biotin signals detected by FITC of anti-biotin antibody using 488-nm excitation and 525-nm emission; middle: GLP-1 signals detected by anti-GLP-1 antibody using 594-nm excitation and 617-nm emission; right: Förster resonance energy transfer (FRET) signals detected using 488-nm excitation and 617-nm emission. Dotted lines delimit the ileal myenteric layer.

(L) Confocal imaging of tissue collected 10 min after intra-ileal infusions of GFP-conjugated-Ex4 in ChAT-ires-Cre×Ai9 reporter mice. GFP was detected in the ileum villa, in the submucosa, and in the myenteric layer as labeled by ChAT+ neurons. Dotted lines delimit the ileal myenteric layer.

(M) Chemogenetic activation of ileal GLP-1R+ neurons induces Fos in the ileal, but not in jejunal, GLP-1R+ neurons; in parentheses are shown the numbers of cells per mm^2. Ileum versus jejunum Fos counts comparisons: Fos+GLP1r−, paired t test T(4) = 2.828, p = 0.047; Fos-GLP1r+, T(4) = 1.000, p = 0.374; Fos+GLP1r+ T(4) = 15.377, * p < 0.001.

(N) GLP-1^{icv}, but not GLP-1^{ii} induce Fos expression in GLP-1R+ neurons of the *area postrema* (AP). Both GLP-1^{icv} and GLP-1^{ii} induce Fos in GLP-1R+ neurons of *nucleus tractus solitarius* (NTS). Right: Fos+ counts in NTS 2-sample t test T(4) = 2.088, p = 0.105; AP, T(4) = 14.584, * p < 0.001.

(O) GLP-1^{ii} induces Fos expression in NTS and AP, GLP-1^{ii} versus Saline^{ii}; NTS, 2-sample t test T(4) = 11.917, * p < 0.001; AP T(4) = 6.426, ** p = 0.003.

(P) GLP-1^{ii} does not induce robust flavor aversion, pre versus post GLP-1^{ii}-paired flavor preference, paired t test, T(4) = 2.432, p = 0.072.

(Q) GLP-1^{icv} induces a slightly more robust flavor aversion pre versus post GLP-1^{icv}-paired flavor preference, paired t test, T(4) = 3.201, * p = 0.033.

(R) Diphtheria toxin (DTx)-induced ablation of ileal GLP-1R+ neurons disrupted the dose-dependent gastric effects of GLP-1^{ii} at 10, 50, 100 pmol/kg, two-way mixed RM-ANOVA, infusate: F(2,16) = 32.363, * p < 0.001; group: F(1,8) = 220.714, * p < 0.001; infusate × group F(2,16) = 8.934, * p = 0.002.

(S) Diphtheria toxin (DTx)-induced ablation of ileal GLP-1R+ neurons disrupted NTS Fos expression induced by GLP-1^{ii}, at 10, 50, 100 pmol/kg, Fos+ counts in NTS two-way mixed RM-ANOVA, infusate: F(2,8) = 32.32, * p < 0.001; Group: F(1,4) = 65.918, * p = 0.001; infusate × group F(2,8) = 7.282, * p = 0.016. Fos+ counts in AP two-way mixed RM-ANOVA, infusate: F(2,8) = 2.981, p = 0.108; group: F(1,4) = 0.481, p = 0.526; infusate × group F(2,8) = 1.17, p = 0.358.

(T) AAV5-flex-Casp3 was injected in AP of GLP-1R-ires-*Cre* mice for local ablation of GLP-1R+ neurons (controls injected with AAV5-DIO EYFP). AP GLP-1R ablation failed to abolish the effects of GLP-1^{ii} on stomach enlargement, stomach volumes (mL), GLP-1^{ii} versus Saline^{ii}, 2-sample t test T(8) = 0.469, p = 0.651.

(U) AP GLP-1R ablation failed to abolish the anorectic effects of GLP-1^{ii}: GLP-1^{ii} versus Saline^{ii} 1 h-intake two-way mixed RM-ANOVA, infusate: F(2,16) = 146.825, * p = 0.001; group: F(1,8) = 0.185, p = 0.679; infusate × group F(2,16) = 3.980, * p = 0.040.

(V) Chemogenetic (CNO) activation of ileal GLP-1R+ neurons triggers Fos in NTS (GLP-1R-Gs injected in the ileum with AAVdj-DIO-Gs-mCherry, GLP-1R-Ctrl with AAVdj-DIO-mCherry). NTS 2-sample t test, T(4) = 7.865, * p = 0.001. AP, T(4) = 0.246, p = 0.818. Data are represented as mean ± SEM in all figures.

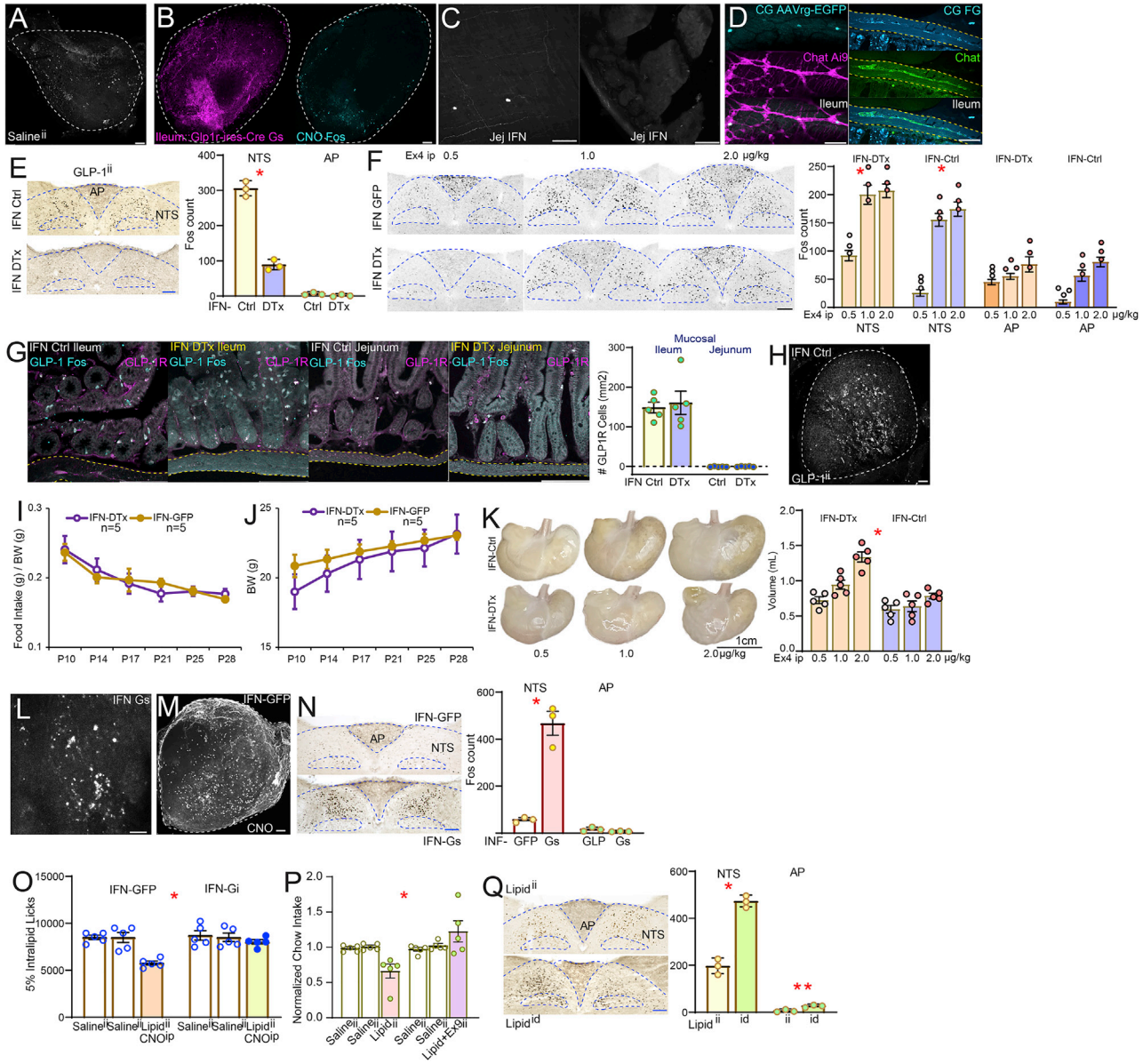

Figure S2. Intestinofugal myenteric neurons mediate the effects of ileal GLP-1, related to Figure 2

(A) Saline^{ii} does not induce Fos in CG.

(B) Unlike CNO, saline injections fail to induce Fos in CG. Note mCherry+ terminals from GLP-1R+ ileal neurons innervating CG.

(C) Retrograde labeling from CG fails to detect intestinofugal neurons in the jejunum.

(D) Left: injection of AAVrg-EGFP into CG of ChAT−ires−*Cre* × Ai9 mice revealed that ileal IFNs are cholinergic myenteric neurons. Right: similar results were obtained by injecting retrograde dye fluorogold (FG) into CG of WT mice followed by antibody staining against ChAT. Dotted lines delimit the ileal myenteric layer.

(E) IFN ablation abolishes Fos expression in NTS but not AP, IFN-DTR-Ctrl versus IFN-DTR-DTx, 2-sample t test NTS $T(4) = 14.363$, * $p < 0.001$, AP $T(4) = 1.780$, $p = 0.15$.

(F) Intra-peritoneal injections of 0.5, 1.0, and 2.0 µg/kg Exendin-4 (Ex4^{ip}) induced Fos expression in NTS and AP of both IFN-DTR-Ctrl and IFN-DTR-DTx mice, IFN-DTR-Ctrl versus IFN-DTR-DTx, two-way mixed RM-ANOVA, NTS: Ex4^{ip} dose $F(2,8) = 80.438$, $p < 0.001$, group $F(1,4) = 21.633$, $p = 0.01$, Ex4^{ip} dose × group $F(2,8) = 1.109$, $p = 0.376$, AP: Ex4^{ip} dose $F(2,8) = 17.829$, $p = 0.001$, group $F(1,4) = 2.425$, $p = 0.194$, Ex4^{ip} dose × group $F(2,8) = 3.309$, $p = 0.09$.

(G) IFN ablation does not affect the number of mucosal GLP-1R+ cells in either ileum or jejunum; IFN-Ctrl versus IFN-DTx, two-way mixed RM-ANOVA, intestinal site × group $F(1,16) = 0.126$, $p = 0.728$.

(H) Fos expression in CG remains robust after GLP-1^{ii} in IFN-DTR-Ctrl mice. Dotted lines delimit myenteric layers.

(I) IFN ablation does not affect food intake (norm. Body weight) under baseline conditions, two-way mixed RM-ANOVA, group: $F(1,10) = 0.000$, $p = 0.989$, time × group $F(4,40) = 2.721$, $p = 0.043$.

(J) IFN ablation does not affect body weight under baseline conditions, two-way mixed RM-ANOVA, group: $F(1,8) = 0.250$, $p = 0.630$, time × group $F(5,40) = 3.416$, $p = 0.012$.

(legend continued on next page)

(K) As in (F), intra-peritoneal injections of 0.5, 1.0, and 2.0 μg/kg Exendin-4 ($Ex4^{ip}$) produced gastric distensions in IFN-DTR-Ctrl mice in a dose-dependent manner, but not in IFN-DTR-DTx mice, IFN-DTR-Ctrl versus IFN-DTR-DTx, two-way mixed RM-ANOVA, $Ex4^{ip}$ dose $F(2,16) = 34.36$, $p < 0.001$, group $F(1,8) = 26.763$, $p = 0.001$, $Ex4^{ip}$ dose × Group $F(2,16) = 9.284$ * $p = 0.002$.

(L) As in Figure 1J. AAVrg-Cre was injected into CG of WT mice followed by *Cre*-dependent AAVdj-DIO-Gs-mCherry into terminal ileum for chemogenetic activation of IFNs (IFN-Gs, controls injected with AAVdj-DIO-GFP, IFN-GFP). The panel shows mCherry+ IFN terminals in CG of animals used for chemogenetic activation of IFNs.

(M) Compared with IFN-Gs, IFN-GFP induces significantly weaker Fos expression in CG.

(N) Chemogenetic IFN activation enhances NTS, but not AP, Fos expression, IFN-Ctrl versus IFN-Gs, 2-sample t test NTS, $T(4) = 7.927$, $p = 0.001$; AP, $T(4) = 1.694$, $p = 0.165$.

(O) AAVrg-Cre was injected into CG of WT mice followed by *Cre*-dependent AAVdj-DIO-Gi-mCherry into terminal ileum for chemogenetic inhibition of IFNs (IFN-Gi, controls injected with AAVdj-DIO-GFP, IFN-GFP). CNO injections abolished the anorectic effects of lipid infusions into the ileum (ileal brake, 1 h-food intake), two-way mixed RM-ANOVA, infusate (lipid versus vehicle) × group $F(2,16) = 11.498$, * $p = 0.001$.

(P) Intra-ileal infusions of the GLP-1R antagonist Exendin9-39 block the anorectic effects of intra-ileal lipids, on 1 h-food intake, two-way mixed RM-ANOVA, infusate × group $F(2,8) = 7.083$, * $p = 0.017$.

(Q) Differential effects of intra-ileal or intra-duodenal infusions of lipid on Fos expression in NTS but not AP, 2-sample t test NTS, $T(4) = 11.437$, * $p < 0.001$, AP, $T(4) = 4.510$, ** $p = 0.011$. Data are represented as mean ± SEM in all figures. Scale bars, 100 μM.

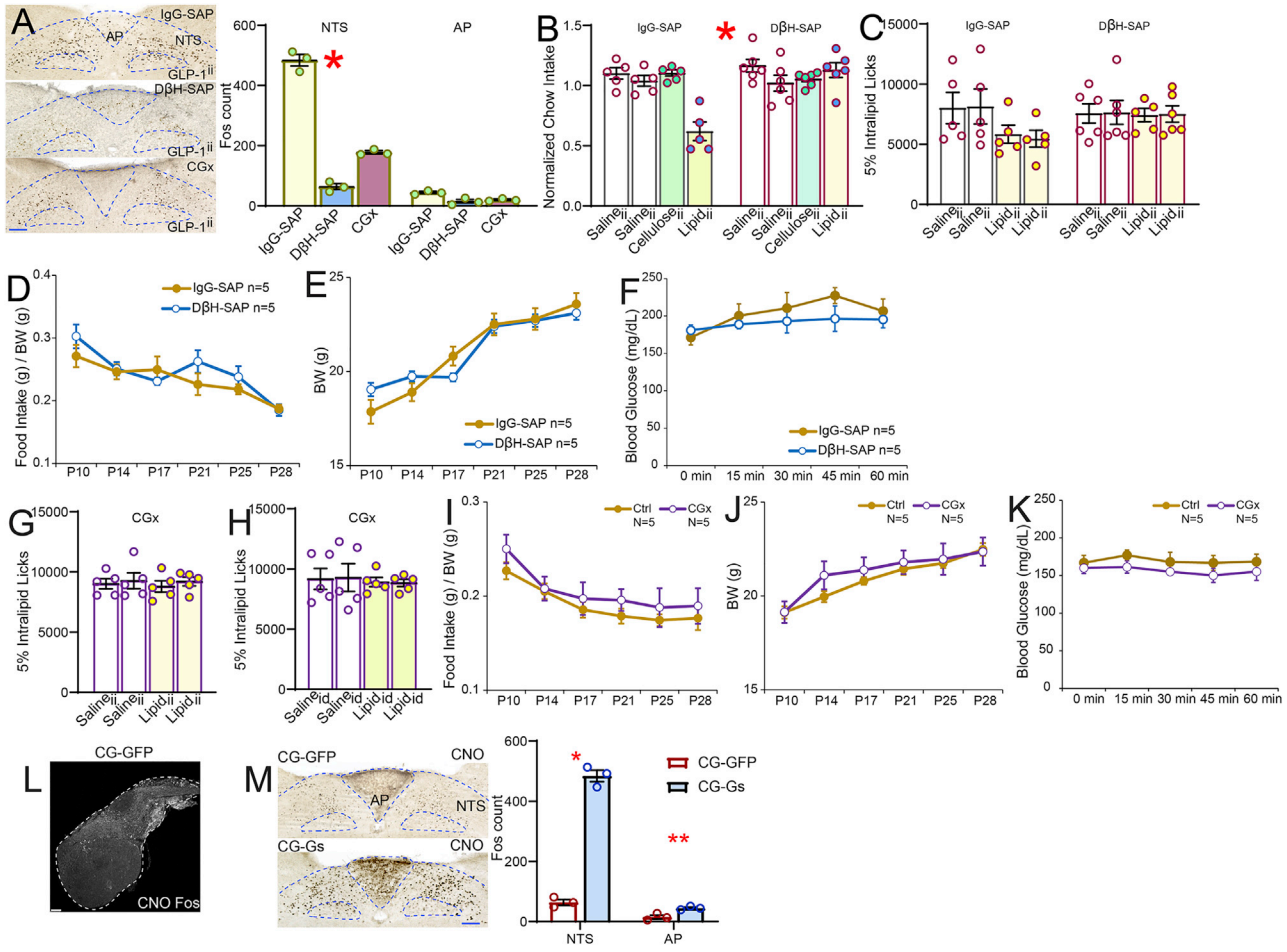

Figure S3. Abdominal (celiac) sympathetic ganglia mediate the effects of ileal GLP-1, related to Figure3

(A) DβH-sap, and less so CGx, disrupt GLP-1^{ii}-induced Fos expression in NTS, one-way ANOVA $F(2,7) = 241.884$, * $p < 0.001$; Bonferroni DβH-sap versus IgG-SAP, $p < 0.001$; DβH-sap versus CGx, $p = 0.003$. No effects in AP, $F(2,7) = 0.509$, $p = 0.622$.

(B) DβH-sap abolishes intra-ileal lipid-induced anorexia, two-way mixed RM-ANOVA, infusate × group $F(3,27) = 13.039$, * $p < 0.001$.

(C) Similar albeit weaker effects for intra-ileal lipid-induced suppression of licks for lipids, infusate: $F(3,27) = 3.170$, $p = 0.040$; group: $F(1,9) = 0.345$, $p = 0.572$, infusate × group: $F(3,27) = 2.263$, $p = 0.104$.

(D) DβH-sap does not affect food intake (norm. Body weight) under baseline conditions, two-way mixed RM-ANOVA, time × group $F(5,40) = 1.185$, $p = 0.334$.

(E) DβH-sap does not affect body weight under baseline conditions, two-way mixed RM-ANOVA, group: $F(1,8) = 0.004$, $p = 0.948$, time × group $F(5,40) = 8.101$, * $p < 0.001$.

(F) DβH-sap does not impact the lack of effects on baseline plasma glucose after GLP-1^{ii}; two-way mixed RM-ANOVA, infusate × group $F(4,32) = 0.484$, $p = 0.747$.

(G and H) CGx abolished intra-ileal (G, one-way RM-ANOVA $F[3,12] = 0.251$, $p = 0.859$) and intra-duodenal (H, $F[3,12] = 0.126$, $p = 0.943$) lipid-induced suppression of lipid licks.

(I) CGx does not affect food intake (normalized to body weight) under baseline conditions, two-way mixed RM-ANOVA, time × group $F(5,40) = 0.669$, $p = 0.649$.

(J) CGx does not affect body weight under baseline conditions, two-way mixed RM-ANOVA, group $F(1,8) = 0.334$, $p = 0.579$, time × group $F(5,40) = 0.936$, $p = 0.468$.

(K) CGx does not affect blood glucose levels under baseline conditions, two-way mixed RM-ANOVA, time × group $F(4,32) = 0.281$, $p = 0.888$.

(L) Saline injections do not induce Fos in CG-Gs mice.

(M) CNO activation of CG^{Stom} robustly induces Fos in NTS (2-sample t test $T[4] = 19.373$, * $p < 0.001$) and AP ($T[4] = 4.058$, ** $p = 0.015$). Data are represented as mean ± SEM in all figures. Scale bars, 100 μM.

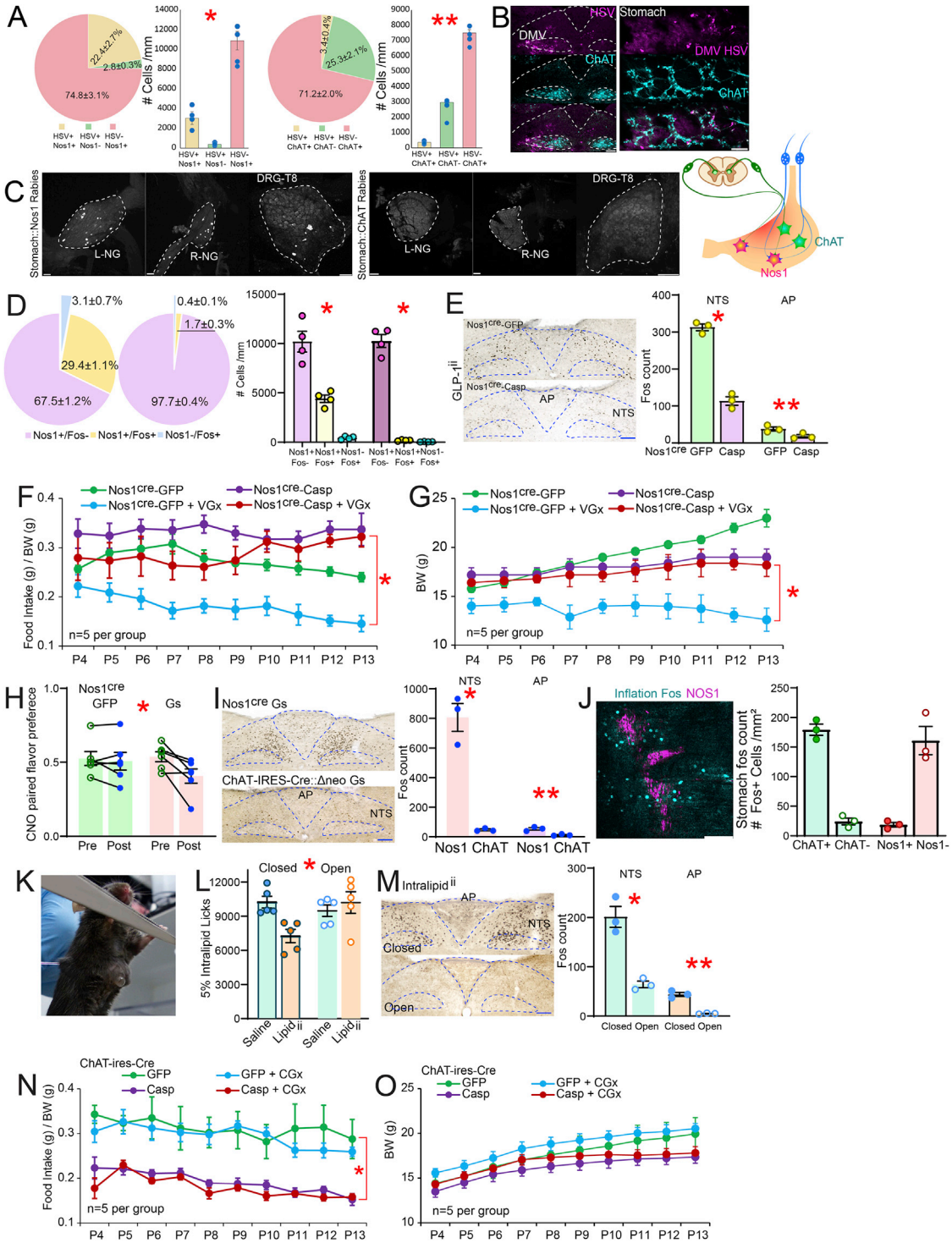

Figure S4. Nos1 and ChAT gastric enteric neurons reciprocally control the effects of ileal GLP-1, related to Figure 4

(A) After gastric infections with the retrograde construct AAVrg-Cre, the polysynaptic, Cre-dependent anterograde Herpes Simplex strain HSV-LSL-TK-Tomato was injected into CG. Recombination of HSV-LSL-TK-Tomato in CG^{Stom} reveals that CG targets mainly Nos1+ (Nos1^{Stom}) gastric neurons, one-way ANOVA, Neuron type F(2,9)= 59.667, ** p < 0.01, and rarely infect ChAT^{Stom} neurons, one-way ANOVA, Neuron type F(2,9)= 183.087, ** p < 0.01.

(B) Injections of the polysynaptic, *Cre*-dependent anterograde *Herpes Simplex* strain HSV-LSL-TK-Tomato into DMV of ChAT-ires-*Cre* mice spread into nearby medullary sites (left) and labels ChAT^{Stom}.

(legend continued on next page)

(C) Left: *Cre*-dependent rabies show that Nos1^{Stom}, not ChAT^{Stom} (middle), are innervated by spinal (dorsal root, DRG) and vagal (nodose, NG) sensory ganglia. Right: scheme depicting rabies results.
(D) GLP-1^{ii}-induced strong and specific Fos in Nos1^{Stom}, an effect abolished by DβH-sap, two-way mixed RM-ANOVA, Neuron type $F(2,12) = 224.839$, $p < 0.001$, group $F(1,6) = 9.983$, $p = 0.02$, neuron type × group $F(2,12) = 11.232$, $p = 0.002$.
(E) Cell-specific ablation (AAV1-flex-Casp3) of Nos1^{Stom} abolishes GLP-1^{ii}-induced Fos expression in both NTS (AAV1-flex-Casp3 versus AAV1-DIO-EYFP, $T[4] = 13.544$, * $p < 0.001$) and AP ($T[4] = 2.865$, ** $p = 0.046$).
(F) Cell-specific ablation (AAV1-flex-Casp3) of Nos1^{Stom} abolishes truncal vagotomies (VGx)-induced anorexia, two-way mixed RM-ANOVA, time × group $F(27,144) = 1.840$, $p = 0.012$, AAV1-DIO-EYFP+VGx versus AAV1-flex-Casp3+VGx Bonferroni * $p = 0.001$.
(G) Cell-specific ablation of Nos1^{Stom} (AAV1-flex-Casp3 in stomach of Nos1^{Cre} mice; controls with AAV1-DIO-EYFP) abolished truncal vagotomy (VGx)-induced body weight loss; two-way mixed RM-ANOVA, time × group $F(27,144) = 7.629$, $p = 0.001$, AAV1-DIO-EYFP+VGx versus AAV1-flex-Casp3+VGx Bonferroni * $p = 0.001$.
(H) Chemogenetic Nos1^{Stom} activation induces mild flavor aversion, two-way mixed RM-ANOVA, infusate × group $F(1,10) = 5.296$, * $p = 0.044$.
(I) Chemogenetic activation of Nos1^{Stom}, not ChAT^{Stom}, induces Fos expression in NTS (Nos1-Gs versus ChAT-Gs, $T[4] = 8.039$, * $p = 0.001$) and AP ($T[4] = 4.704$, ** $p = 0.009$).
(J) Left: gastric balloon inflation infrequently induces stomach Fos expression in Nos1+ neurons; Right: gastric balloon preferentially induced Fos expression in stomach ChAT+, not Nos1+, neurons; two-way mixed RM-ANOVA, Fos activity × neuronal type $F(1,4) = 111.118$, $p < 0.001$.
(K) Implanted gastric fistula in awake behaving mice allows for sham-feeding experiments.
(L) Open fistula abolishes intra-ileal lipid-induced anorexia, two-way RM-ANOVA, main effect of ileal lipid $F(1,4) = 17.358$,* $p = 0.014$.
(M) Open fistula abolishes intra-ileal lipid-induced Fos in NTS (paired t test, open versus closed fistula $T[4] = 7.311$, * $p = 0.002$) and AP ($T[4] = 8.769$, ** $p = 0.001$).
(N) Cell-specific ablation (AAV1-flex-Casp3) of ChAT^{Stom} induces anorexia irrespective of CGx, two-way mixed RM-ANOVA, time × group $F(27,144) = 2.985$, $p < 0.001$, AAV1-DIO-EYFP versus AAV1-flex-Casp3 Bonferroni * $p < 0.001$.
(O) Cell-specific ablation of ChAT^{Stom} (AAV1-flex-Casp3 in the stomach of ChAT-ires-Cre mice; controls with AAV1-DIO-EYFP) induces body weight reductions irrespective of CGx; two-way mixed RM-ANOVA, time × group $F(27,144) = 1.615$, $p = 0.039$. Data are represented as mean ± SEM in all figures. Scale bars, 100 μM.

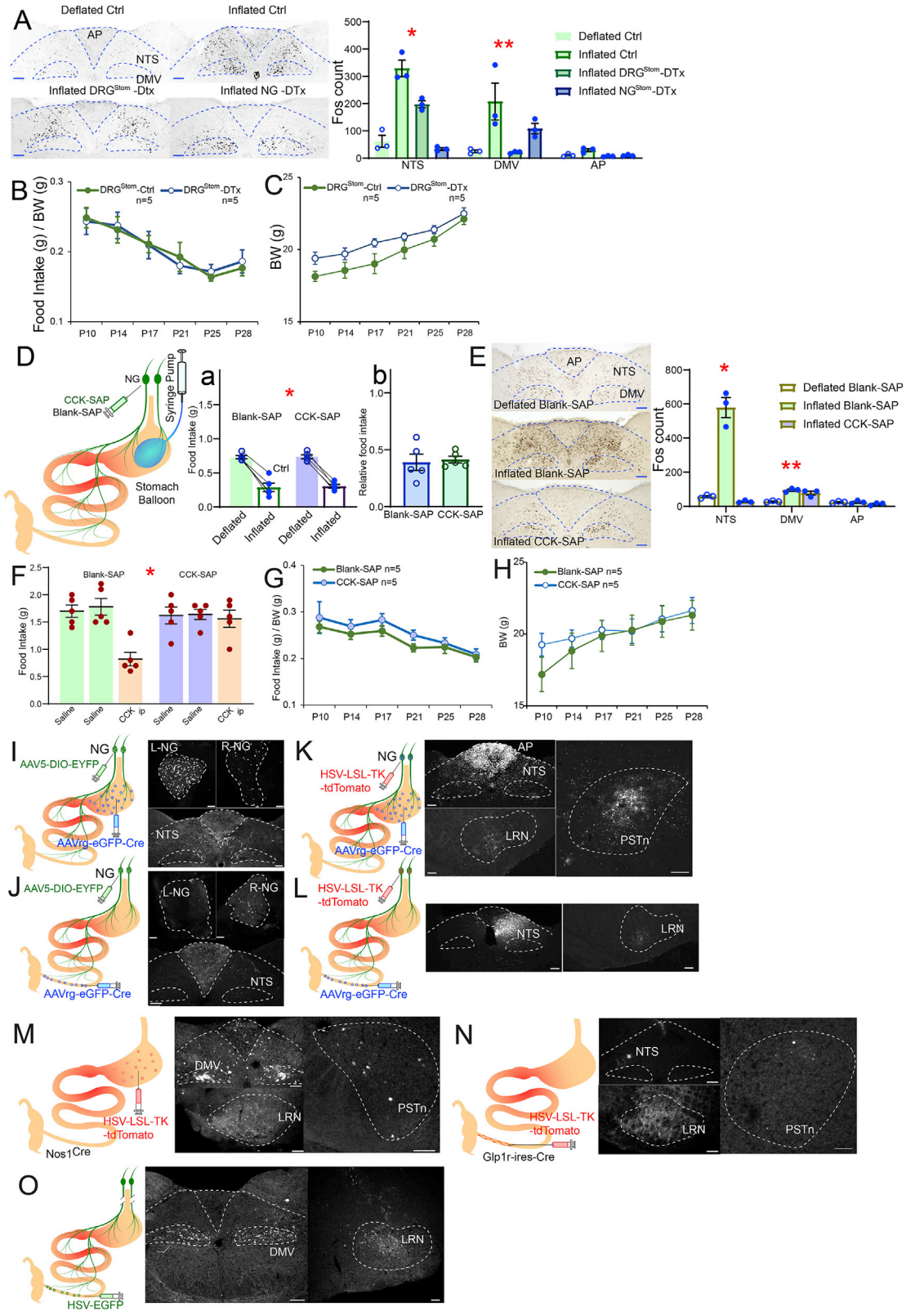

(legend on next page)

Figure S5. Spinal sensory neurons convey the status of stomach distension to the brain, related to Figure 5

(A) DRG^{Stom} ablation suppressed balloon-induced Fos expression in DMV, and NG^{Stom} ablation suppressed balloon-induced Fos expression in NTS, but not in DMV; one-way ANOVA NTS $F(3,8) = 48.046$, * $p < 0.001$, DMV $F(3,8) = 6.186$, ** $p = 0.018$. No effects detected in AP $F(3,8) = 9.886$, $p = 0.005$.

(B) DRG^{Stom} ablation does not affect food intake (norm. body weight) under baseline conditions, two-way mixed RM-ANOVA, time × group $F(5,40) = 0.202$, $p = 0.960$.

(C) DRG^{Stom} ablation does not affect food intake under baseline conditions, two-way mixed RM-ANOVA, time × group $F(5,40) = 0.819$, $p = 0.543$.

(D) Saporin-conjugated cholecystokinin (CCK-SAP) was injected into NG to chemically ablate gut-innervating NG neurons, before tests with gastric balloons. Controls injected with unconjugated saporin (Blank-Sap). No anorexia effects of vagal denervation were detected (Da), chow intake: two-way mixed RM-ANOVA, treatment (inflated versus deflated) × group $F(1,8) = 0.035$, $p = 0.856$, main effects of balloon $F(1,8) = 266.514$,* $p < 0.001$, and group $F(1,8) = 0.054$, $p = 0.822$. (Db) relative change in intake: $T(8) = 0.310$, $p = 0.765$.

(E) However, CCK-SAP suppressed balloon-induced Fos in NTS (one-way ANOVA $F[2,6] = 82.887$, * $p < 0.001$) and DMV (one-way ANOVA $F[2,6] = 21.052$, ** $p = 0.002$). No effects detected for in AP ($F[2,6] = 2.013$, $p = 0.214$).

(F) CCK-SAP abolished satiating effects of i.p. cholecystokinin (CCK), two-way mixed RM-ANOVA, Treatment (CCK versus saline) × group $F(2,16) = 25.535$, * $p < 0.001$.

(G) CCK-SAP does not affect feeding under baseline conditions, two-way mixed RM-ANOVA, time × group $F(5,40) = 1.199$, $p = 0.667$.

(H) CCK-SAP does not affect feeding under baseline conditions, two-way repeated RM-ANOVA, group $F(1,8) = 0.220$, $p = 0.652$, time × group $F(5,40) = 8.408$, $p = 0.003$.

(I) Retrograde *Cre*-expressing AAVrg-EGFP-Cre virus injected into the stomach of wild-type mice followed by injection of *Cre*-dependent AAV5-DIO-EYFP into NG. Upper: Left NG were primarily labeled, with terminals visible in subpostremal NTS (lower).

(J) Similar experiments targeting AAVrg-EGFP-Cre into the ileum revealed much weaker labeling in NG, but right NG were primarily labeled.

(K) As in (I), but HSV-LSL-TK-Tomato injected into NG instead. Strong labeling AP/NTS, weak labeling in LRN and PSTn.

(L) As in (J), but HSV-LSL-TK-Tomato injected into NG instead. Weak labeling NTS and LRN.

(M) HSV-LSL-TK-Tomato injected into the stomachs of Nos1^{Cre} mice revealed strong labeling in DMV (upper), and weak labeling in LRN (lower), and PSTN (right).

(N) HSV-LSL-TK-Tomato injected into the ileum of GLP-1R-ires-*Cre* mice revealed strong labeling in LRN and weak labeling in NTS and PSTn.

(O) In vagotomized mice, *Cre*-independent HSV into the ileum revealed labeling in DMV and LRN. Data are represented as mean ± SEM in all figures. Scale bars, 100 μM.

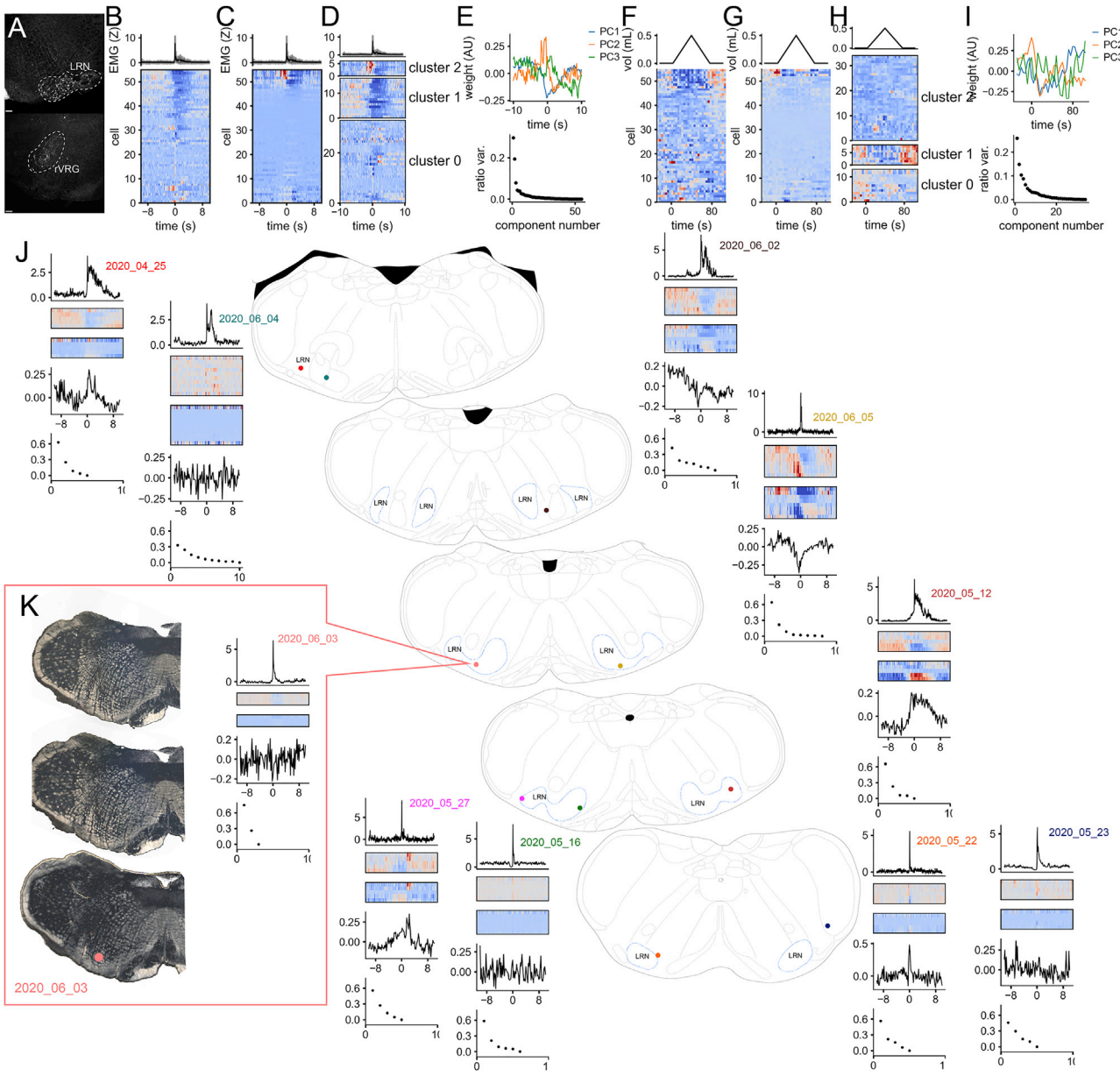

Figure S6. Medullary lateral reticular neurons convey status of stomach distension to the brain, related to Figure 6

(A and B) *Cre*-dependent rabies show that LRN (A) is innervated by neurons located in the rostral ventral respiratory group (rVRG, B).

(B–E) LRN cells are modulated in concert with stomach contraction. (B) LRN cell activity aligned with the initiation of a stomach contraction. The top trace is a triggered average of EMG activity, triggers times are derived from the beginning of the bursts of EMG signal. The initiation of each burst is set to time zero. The heatmap shows the Z-transformed firing rates, in the same row order as the principal component heatmap in (D) in the accompanying main figure. The ordinate in the heatmap is matched to that of the EMG traces and shows the peri-contraction time, negative times are those preceding initiation of stomach contraction, and positive times are following. (C) Heatmap shows principal component PC2 weight for each cell at each time before and after muscle contraction. Upper traces same as (B). (D) Heatmap shows Z-transformed firing rates for each cell, broken in clusters by K means clustering on 3 principal components PC1-3. Not cells inhibited in synchrony with stomach contraction segregate into a different cluster 1 than those which are predominately excited with the contraction. (E) The top line plots show the shape of the first three principal components PC1-3, the lower plot shows the ratio of variation explained by each principal component.

(F–I) A few LRN cells are inhibited during the inflation of a balloon in the stomach. (F) LRN cell activity aligned to the initiation balloon inflation-deflation cycles. The top trace shows balloon volume. The initiation of each burst is set to time zero. The heatmap shows the Z-transformed firing rates, in the same row order as the principal component heatmap in (B) in the accompanying main figure. The ordinate in the heatmap is matched to that of the balloon volume. (G). Heatmap shows principal component PC2 weight for each cell during the balloon inflation program. (H) Similar to (D), but cells rasters are aligned to the balloon program. (I) Similar to E but showing principal component PC2 calculated on responses to balloon program.

(J) Responsivity mapping of LRN neurons recorded at different sites within LRN. Each recording session is indicated by a colored dot, and the accompanying data in the same color labels a column of 4 plots. The top plot shows the burst-triggered EMG signal for this experiment. The upper heatmap in each column shows the

(legend continued on next page)

Z-transformed firing rates for the cells recorded in this session. The lower heatmap shows the principal component PC1 weight. Principal component analysis was performed separately for each set of neurons recorded in a single experiment. The lower line plot shows the shape of the first principal component, and the lowest plot in the column, shows the ratio of explained variance. Note that site 2020_05_23 was excluded from the analysis shown in the main figure (mistarget). (K) Representative histological determination of recording site 2020_06_03. Data are represented as mean ± SEM in all figures. Scale bars, 100 μM.

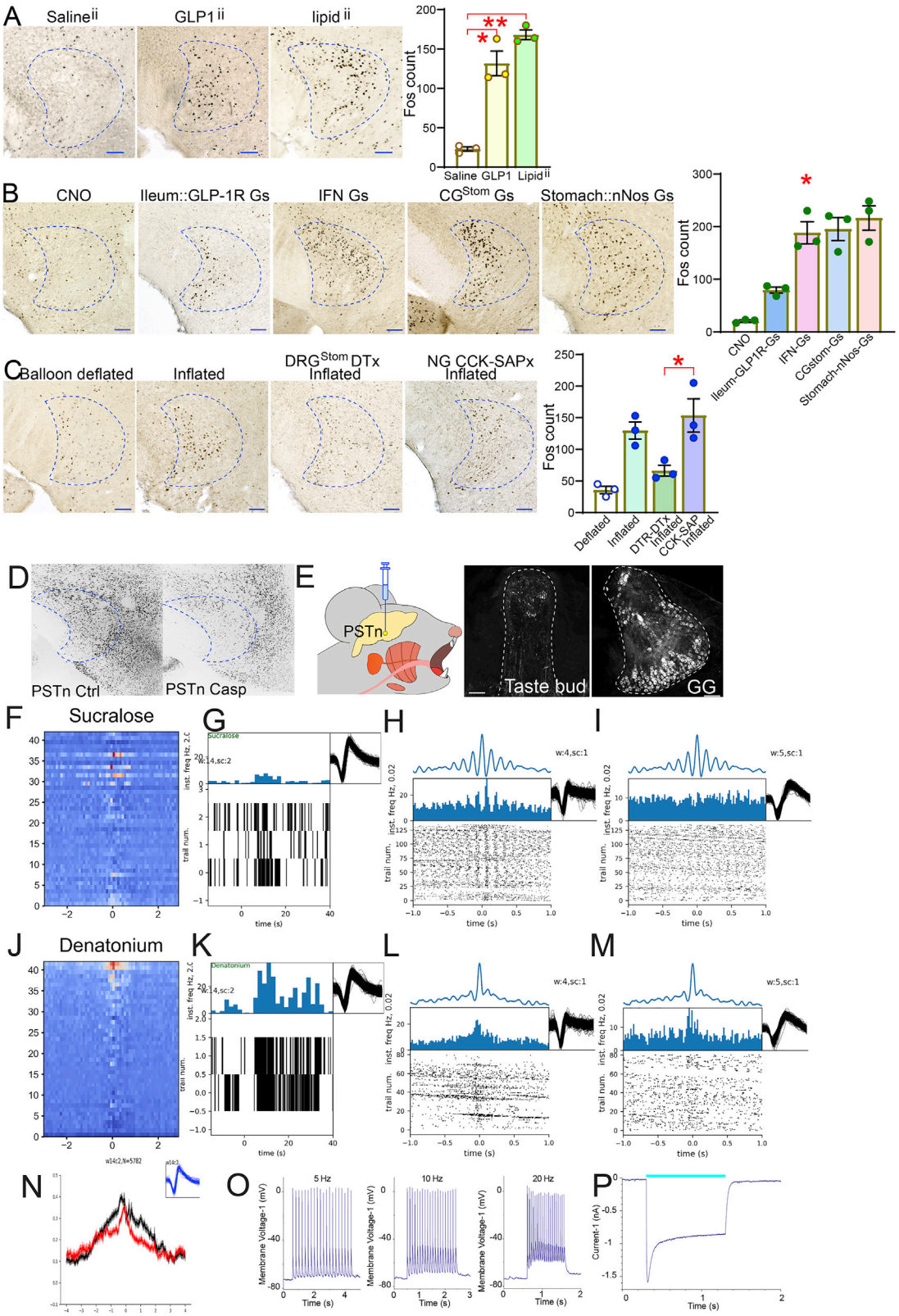

(legend on next page)

Figure S7. Glutamatergic neurons in the parasubthalamic hypothalamus control the effects of ileal GLP-1, related to Figure 7

(A) Both GLP-1^{ii} and Lipid^{ii} induce robust Fos expression in PSTn, one-way ANOVA $F(2,6) = 58.661$, $p < 0.001$, GLP-1^{ii} versus Saline^{ii} followed by post-hoc correction Bonferroni * $p = 0.001$; Lipid^{ii} versus Saline^{ii} Bonferroni ** $p < 0.001$.

(B) Chemogenetic activation of INF^{Stom} (INF-Gs), CG^{Stom} (CG-Gs), and Nos1^{Stom} (Nos1-GS) all induce Fos expression in PSTn; one-way ANOVA $F(4,10) = 24.436$, $p < 0.001$. Post-hoc Bonferroni CNO versus INF-Gs, CG-Gs, Nos1-Gs all * $p < 0.001$; GLP-1R-Gs versus CNO $p = 0.372$.

(C) Intra-gastric balloon inflation induces strong Fos expression in PSTn, and this effect was greatly attenuated by DRG^{Stom} ablation (DRGx^{Stom}) but not by NG ablation upon CCK-SAP injections in NG: one-way ANOVA $F(3,8) = 12.185$, $p = 0.002$. Inflated-DRGx^{Stom} versus inflated-CCK-SAP Bonferroni * $p = 0.026$. Scale bars, 100 μM.

(D) *Cre*-dependent Casp3 induced PSTn^{VGlut2} lesions as confirmed via NeuN immunolabeling.

(E) PRV-DIO-TK-GFP injected into PSTn^{VGlut2} neurons labeled neurons in taste buds and taste geniculate ganglia (GG).

(F) Heatmap of the first principal component for 42 units recorded in the PSTn, aligned to digastric EMG bursts that were elicited after intra-oral infusions of sucralose, 2 out of 42 units are significantly modulated, and one overlaps with the denatonium set in (J).

(G) Taste reactivity trials showing the firing rate of a PSTn unit that weakly responded to sucralose.

(H and I) Two different PSTn units are moderately active during digastric contractions (blue traces on top) after infusions of sucralose.

(J) As in (F), except digastric activity is elicited by intra-oral infusions of denatonium, 4 out of 42 units were significantly modulated in concert with digastric activity following the denatonium infusions.

(K) Taste reactivity trials showing the firing rate of a PSTn unit that responded preferentially to denatonium.

(L and M) Two different PSTn units are strongly active during digastric contractions (blue traces on top) after infusions of denatonium.

(N) Spike-triggered average of digastric (black) and masseter (red) electromyogram signals based on the spike times of a denatonium-responsive unit. Note the close relationship between jaw muscle and PSTn activities.

(O) Action potentials (current clamp) from ChR2-expressing PSTn^{VGlut2} neurons upon 5, 10, and 20 Hz optogenetic stimulation.

(P) Inward membrane current recorded in ChR2-expressing PSTn^{VGlut2} neurons under voltage clamp. Blue bar, application of the LED-generated blue light pulse.

Data are represented as mean ± SEM in all figures. Scale bars, 100 μM.